

2D Titanium Carbide/Reduced Graphene Oxide Heterostructures for Supercapacitor Applications

Adriana M. Navarro-Suárez^{+, [a, b]}, Kathleen Maleski,^[a] Taron Makaryan,^[a] Jun Yan,^[a, c] Babak Anasori,^[a] and Yury Gogotsi^{*[a]}

Solution-processable two-dimensional (2D) materials offer the possibility of manufacturing heterostructures with various properties, creating a way to tune materials towards a specific application. Two different 2D materials, titanium carbide MXene ($Ti_3C_2T_x$) and reduced graphene oxide (rGO), have shown promising results for supercapacitor applications due to their flake-like morphology, high conductivity; and ability to intercalate molecules or ions for charge storage. Here, we demonstrate the self-assembly of a heterostructure between negatively charged $Ti_3C_2T_x$ and positively charged modified rGO after shear

mixing. Changes in zeta (ζ) potential, X-ray diffraction (XRD) patterns; and Raman spectra confirm the assembly of this heterostructure. The produced rGO: $Ti_3C_2T_x$ heterostructures were used as electrodes for supercapacitors. The addition of rGO to $Ti_3C_2T_x$ allowed some widening of the voltage window. Moreover, due to the synergistic effect of these materials, an increase of the capacitance value was observed. An electrode film composed of rGO (1 wt.%) and $Ti_3C_2T_x$ (99 wt.%) achieved capacitance values up to $254\text{ F}\cdot\text{g}^{-1}$ at $2\text{ mV}\cdot\text{s}^{-1}$ and $193\text{ F}\cdot\text{g}^{-1}$ at $100\text{ mV}\cdot\text{s}^{-1}$.

1. Introduction

Current energy storage devices are based on the capture and release of metal ions and electric charges, i.e. batteries and supercapacitors.^[1] These can be found in several configurations, dimensions, and can contain many types of materials, but the current technology relies on particulate-like nanomaterials, which may lose their mechanical integrity upon bending.^[2] In contrast, two-dimensional (2D) materials are inherently flexible and have a high surface reactivity, high electrical conductivity, and large surface area, which are fundamental characteristics of energy storage devices. The exfoliation of graphite into single layers of graphene, in 2004, resulted in a new explosion of interest in 2D materials.^[3] A large family of 2D transition metal carbides and nitrides, called MXenes, are gaining interest in a variety of applications due to their promising properties.^[4,5] MXenes have a general formula of $M_{n+1}X_nT_x$, where M is an early transition metal (e.g., Ti, Nb, V, Mo), X can be carbon or

nitrogen, n is equal to 1, 2 or 3 and T_x represents surface functional terminations such as –OH, –O, or –F. The 2D structures are made of sheets of transition metals that are interleaved with sheets of carbon or nitrogen in a $[MX]_nM$ arrangement.^[5]

Stacking two-dimensional materials, such as graphene and MXene, can be made into layered heterostructures.^[6–8] This architecture leads to the possibility of creating and designing layered artificial structures with “on-demand” properties, making them of notable interest for a range of applications, including energy storage.^[1,9] A 3D heterostructure constructed from MXene and rGO could have the potential to stop aggregation and restacking of MXene or rGO nanosheets, which has been demonstrated to deteriorate the intrinsic electrochemical performance of the 2D materials.^[10]

Titanium carbide MXene ($Ti_3C_2T_x$) and reduced graphene oxide (rGO) are 2D materials which have shown promising results in supercapacitors devices.^[5,11–16] So far, there are two reports on the assembly of stacked structures of titanium carbide/rGO heterostructures.^[17,18] However, designing a homogeneous and uniform heterostructure comprising these two materials is a challenge given that $Ti_3C_2T_x$ and rGO are both negatively charged. To achieve a self-assembled layered structure with two inherently negatively charged materials, surface functionalization can be used to alter the surface charges of the 2D sheets. Recently, we reported a strategy to prepare $Ti_3C_2T_x$ /rGO films by using electrostatic self-assembly between positively charged rGO with poly(diallyldimethylammonium chloride) (PDDA) and negatively charged $Ti_3C_2T_x$ MXene nanosheets. After electrostatic assembly, rGO nanosheets were inserted in between $Ti_3C_2T_x$ layers.^[19]

Here, we show that functionalizing rGO with amine groups can effectively change the surface charge on rGO from negative to positive. Thus, when the positively charged rGO nanosheets

[a] Dr. A. M. Navarro-Suárez,⁺ K. Maleski, Dr. T. Makaryan, Dr. J. Yan, Dr. B. Anasori, Prof. Y. Gogotsi

Department of Materials Science & Engineering and A.J. Drexel Nanomaterials Institute, Drexel University Philadelphia, PA 19104, USA

E-mail: gogotsi@drexel.edu

[b] Dr. A. M. Navarro-Suárez⁺

CIC energiGUNE
Albert Einstein 48, 01510 Miñano, Alava, Spain

[c] Dr. J. Yan

Key Laboratory of Superlight Materials and Surface Technology, Ministry of Education, College of Material Science and Chemical Engineering Harbin Engineering University Harbin 150001, China

[+] Current address: Department of Physics, Chalmers University of Technology, 41296 Gothenburg, Sweden

 Supporting Information and the ORCID identification number(s) for the author(s) of this article can be found under: <https://doi.org/10.1002/batt.201800014>

are mixed with negatively charged $\text{Ti}_3\text{C}_2\text{T}_x$, a self-assembly takes place, resulting in a 3D heterostructure comprised of $\text{Ti}_3\text{C}_2\text{T}_x$ and rGO. By fabricating this heterostructure, we achieved an increase in the potential window of $\text{Ti}_3\text{C}_2\text{T}_x$ up to 0.7 V while simultaneously increasing the capacitance values, suggesting that $\text{Ti}_3\text{C}_2\text{T}_x$ /rGO heterostructures can be beneficial for supercapacitor electrodes and other applications.

2. Results and Discussion

The scheme shown in Figure 1 illustrates the synthesis method of the flexible rGO: $\text{Ti}_3\text{C}_2\text{T}_x$ heterostructured films. Reduced graphene oxide and $\text{Ti}_3\text{C}_2\text{T}_x$ MXene are both inherently negatively charged on their surface.^[20,21] To achieve a self-assembled heterostructure, reduced graphene oxide was functionalized with amine groups and then mixed with $\text{Ti}_3\text{C}_2\text{T}_x$ MXene. When the solutions were mixed, the positively charged NH_2 -rGO interacted with the negatively charged $\text{Ti}_3\text{C}_2\text{T}_x$. It has been proven that shear mixing provides good dispersion and can help during intercalation processes depending on the surface modification of the initial materials.^[22]

By measurement of the isoelectric point (IEP), information about the surface charge as a function of a solution pH can be obtained.^[23] At a given IEP, the zeta (ζ)-potential reaches a 0 mV value. The pH value where the ζ -potential crosses the IEP can be used to compare one material's surface (i.e., surface functional groups) to another material. Figure 2 shows the ζ -potential scaling with pH for solutions of $\text{Ti}_3\text{C}_2\text{T}_x$, NH_2 -rGO, and various rGO: $\text{Ti}_3\text{C}_2\text{T}_x$ mixtures. Comparing non-mixed solutions, the IEP of $\text{Ti}_3\text{C}_2\text{T}_x$ appears at a pH value of 2.45 whereas NH_2 -rGO has an IEP at a pH value of 8.85, displaying the differences in the negatively charged surface of $\text{Ti}_3\text{C}_2\text{T}_x$ compared to the positively charged surface of NH_2 -rGO. In the rGO: $\text{Ti}_3\text{C}_2\text{T}_x$ mixtures, the ζ -potential became more positive at each respective pH value and the isoelectric point shifted to higher pH with increasing content of rGO.

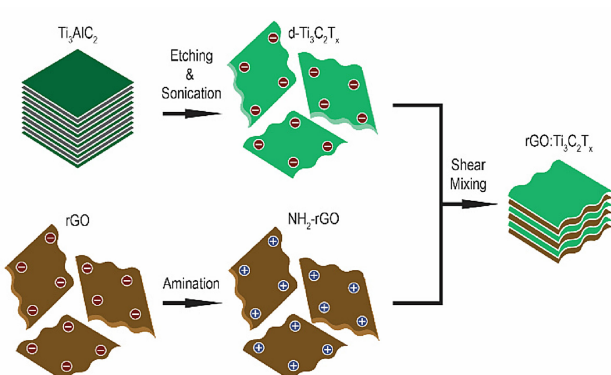


Figure 1. Scheme illustrating the various steps involved in the manufacturing of the rGO: $\text{Ti}_3\text{C}_2\text{T}_x$ heterostructure films. d- $\text{Ti}_3\text{C}_2\text{T}_x$ was synthesized by etching MAX phase, Ti_3AlC_2 , and delaminated by sonication. Functionalized rGO was prepared by amination of rGO at 80 °C to create NH_2 -rGO. Both d- $\text{Ti}_3\text{C}_2\text{T}_x$ and NH_2 -rGO were shear mixed and filtered to form a 2D heterostructure.

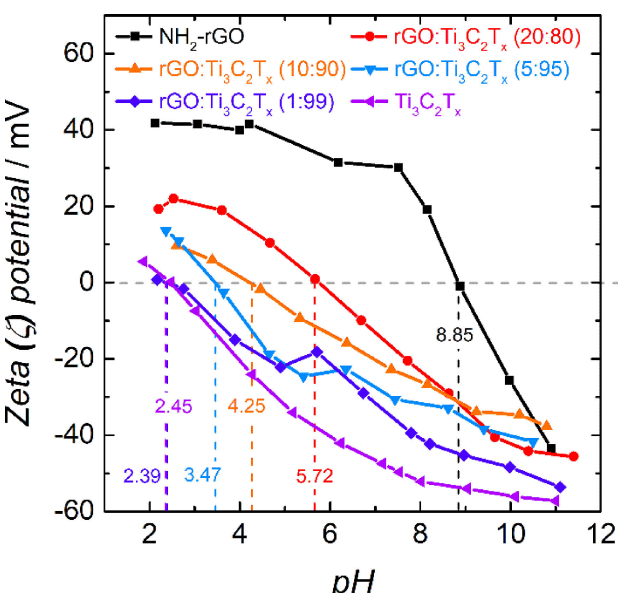


Figure 2. Evolution of the ζ -potential with respect to pH of the different mixtures. The numbers denote the IEP of each sample. The IEP shifts to higher pH with increasing rGO content.

The morphology of the films obtained by vacuum-assisted filtration were characterized by SEM. While the filtration of NH_2 -rGO only lead to clusters of the material and no film was obtained, filtration of the MXene containing solutions led to freestanding films. A representative cross-sectional image (Figure 3) shows that all the films had layered structures similar to the morphologies exhibited by $\text{Ti}_3\text{C}_2\text{T}_x$ ^[21] and rGO^[20] films. The EDX spectroscopy (Table S1) performed on the heterostructures confirmed that the titanium percentage decreased with increasing NH_2 -rGO content.

Figure 4a shows the Raman spectra of the d- $\text{Ti}_3\text{C}_2\text{T}_x$, NH_2 -rGO, and different rGO: $\text{Ti}_3\text{C}_2\text{T}_x$ hybrid films. The rGO: $\text{Ti}_3\text{C}_2\text{T}_x$ hybrids presented characteristics typical of both d- $\text{Ti}_3\text{C}_2\text{T}_x$ and rGO. The four broad Raman peaks centered around 199.5, 369,

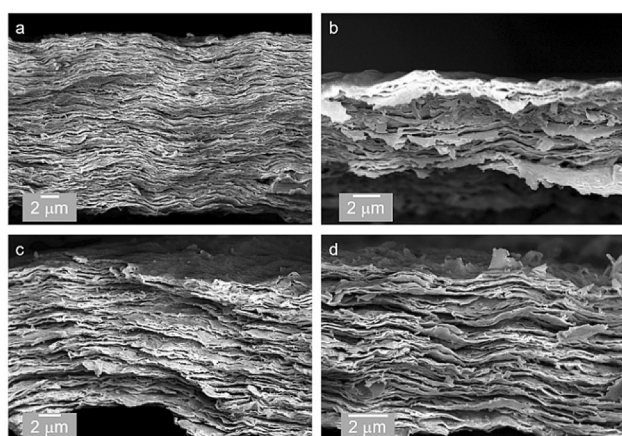


Figure 3. SEM cross-sectional image of the rGO: $\text{Ti}_3\text{C}_2\text{T}_x$ films with different volume ratios of (a) 20:80, (b) 10:90, (c) 5:95 and (d) 1:99, showing the layered structure is kept in all the composites.

628.5 and 716.3 cm^{-1} are attributed to the vibrations from non-stoichiometric titanium carbide.^[24] Namely, the first two (199.5

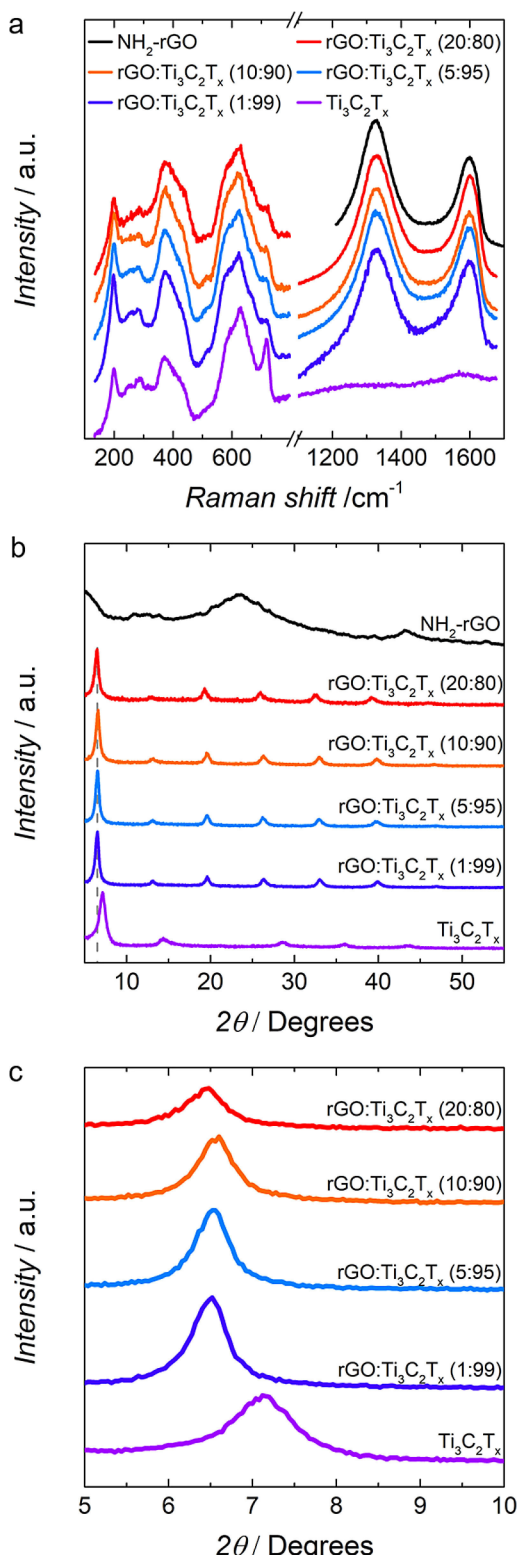


Figure 4. Raman (a), XRD patterns (b) and zoomed-in (002) peak region (c) of the d-Ti₃C₂T_x, NH₂-rGO, and different rGO:Ti₃C₂T_x hybrid films at different rGO:Ti₃C₂T_x ratios. The heterostructures presented characteristics typical of both d-Ti₃C₂T_x, and rGO.

and 369 cm^{-1}) are from A_{1g} and E_g symmetry Ti–C and O vibrations, respectively.^[25] The latter two (628.5 and 716.3 cm^{-1}) are ascribed to the C atoms E_g and A_{1g} symmetry vibrations of mostly –O and –OH terminated groups.^[25] The shift generated in the Raman peaks in comparison with pure d-Ti₃C₂T_x, especially, of the 716.3 cm^{-1} band, can be ascribed to the change of the functional groups.^[25] At higher wavenumbers, the D and G bands, typical of graphene, can be observed. The G peak (1595 cm^{-1}) corresponds to the high-frequency E_{2g} phonon at the Γ -point. The D peak (1331 cm^{-1}) is due to the breathing modes of six-atom rings and requires a defect for its activation.^[26] Raman results show that rGO and Ti₃C₂T_x kept their structure, even when constructed as heterostructures.

To study the change in the interlayer distances caused by the inclusion of rGO inside the Ti₃C₂T_x layers, we studied the X-ray diffraction (XRD) patterns of d-Ti₃C₂T_x, NH₂-rGO, and the different rGO:Ti₃C₂T_x hybrid films (Figure 4b). NH₂-rGO has a stochastic (002) peak in the range from 18.9 to 29.3° (top pattern in Figure 4b), corresponding to water-filled space between the layers, which fluctuated between 3 and 4.7 Å. However, d-Ti₃C₂T_x showed a sharp, intense (002) peak and higher-order (00l) peaks ascribed to the restacking of Ti₃C₂T_x flakes. The (002) peak ~7.1 corresponds to a c-lattice parameter of 25 Å and an interlayer distance of 12.5 Å.

In the heterostructured electrodes, the lack of the (002) diffraction peak of the NH₂-rGO indicated the absence of periodicity, suggesting that NH₂-rGO nanosheets did not restack during the assembly.^[22] Figure 4c shows that for all the compositions, the (002) peak corresponding to the restacking of the MXene flakes was shifted to 6.5, corresponding to an increased interlayer distance of 13.6 Å, possibly due to the presence of graphene sheets between the Ti₃C₂T_x layers, which agrees with our previous study.^[19] In that study, we showed the alternating single layers of Ti₃C₂T_x and rGO in cross-sectional transmission electron microscopy images.

The layer ratio of Ti₃C₂T_x and rGO was calculated by considering their theoretical specific surface area of single layer of 483.94 and 2630 $\text{m}^2 \cdot \text{g}^{-1}$, respectively,^[19] as presented in Table S2. Our calculations revealed that in rGO:Ti₃C₂T_x (20:80), there were more rGO flakes compared to Ti₃C₂T_x flakes. When the proportion of rGO was decreased to 10 wt.%, there was approximately 1 layer of rGO for every 1–2 layers of Ti₃C₂T_x. As the content of rGO was decreased further to rGO:Ti₃C₂T_x (5:95), 3–4 layers of Ti₃C₂T_x in between each layer of rGO was calculated. The rGO content was decreased until there was approximately 1 layer of rGO for every 18–19 layers of Ti₃C₂T_x in rGO:Ti₃C₂T_x (1:99).

MXenes have shown great potential as electrode materials in supercapacitors.^[14,21,27,28] Pristine, d-Ti₃C₂T_x, has achieved capacitance values up to 238 $\text{F} \cdot \text{g}^{-1}$ in 1 M H₂SO₄.^[28,29] We measured the performance of the various rGO:Ti₃C₂T_x heterostructure films in a three-electrode configuration in 1 M H₂SO₄ as shown in Figure 5. The cyclic voltammetry testing (Figure 5a) showed a typical capacitive behavior within a potential window up to 0.9 V, which was larger than that of the d-Ti₃C₂T_x alone (restricted to 0.55 V). The increase in the voltage window of rGO:Ti₃C₂T_x films can be explained by the inclusion of rGO into

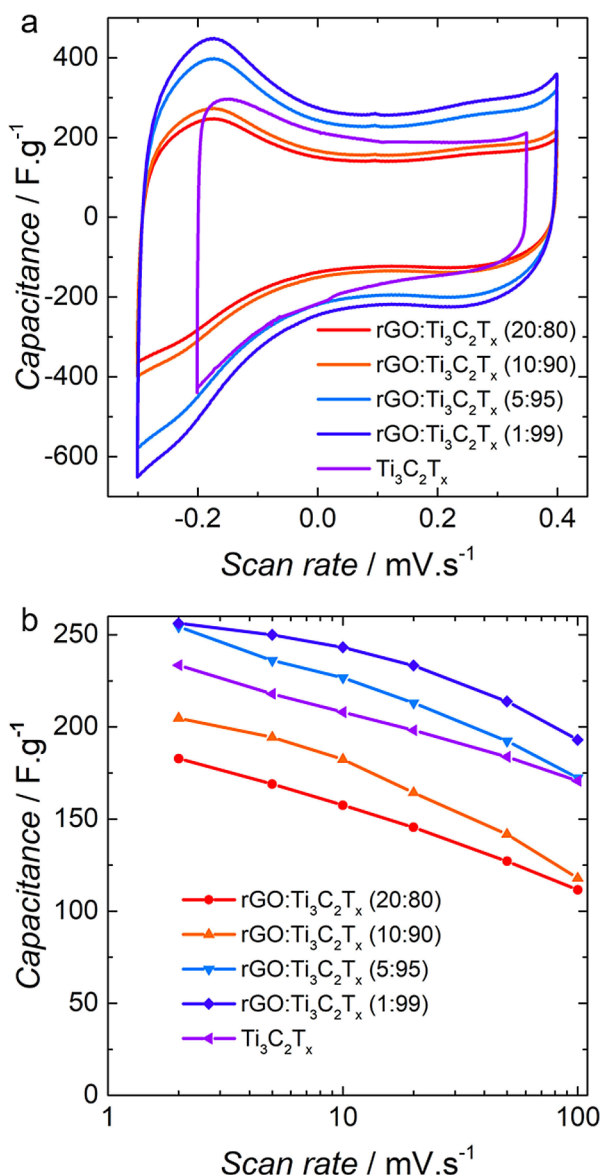


Figure 5. Cyclic voltammetry testing (a) and evolution of the capacitance with scan rate (b) for different rGO:Ti₃C₂T_x samples. d-Ti₃C₂T_x is shown as comparison. The voltage window of the heterostructures is enlarged due to the inclusion of rGO into the Ti₃C₂T_x layers.

the Ti₃C₂T_x layers, allowing for an increase in interlayer spacing, improving ion diffusion and therefore enhancing the electrochemical properties of MXene electrodes.

The improvement in the capacitance with scan rate (Figure 5b) shows that up to 5 wt.% rGO in the heterostructure (1 layer of rGO for every 3–4 layers of Ti₃C₂T_x) proved to be beneficial as the heterostructures achieved capacitance values

up to 256 and 254 F·g⁻¹ at 2 mV·s⁻¹ for 1 and 5 wt.% of rGO, respectively. When the percentage of rGO was increased to values above 5 wt.%, the capacitance decreased below the values exhibited by pristine d-Ti₃C₂T_x. At high scan rates, rGO:Ti₃C₂T_x (1:99) showed the best capacitance retention achieving 193 F·g⁻¹ at 100 mV·s⁻¹. These values of capacitance and capacitance retention could be related to the conductivity of the films shown in Table 1. As the percentage of rGO increased in the films, the electrical conductivity decreased in comparison with pristine d-Ti₃C₂T_x.^[19] Even though it was not possible to obtain a high-quality NH₂-rGO film, we expect that the conductivity of this material should be higher than that of the rGO modified with PDDA. In NH₂-rGO, nitrogen acts as electron donor significantly increasing the charge carrier density in the basal plane,^[30] and the sp² conjugated basal plane of graphene sheet is restored and the conductivity is enhanced as a result of removing oxygen-containing functional groups.^[31]

The effect of film conductivity could also be observed during impedance measurements of different film electrodes in 1 M H₂SO₄ (Figure 6). At low frequency, all the films behaved

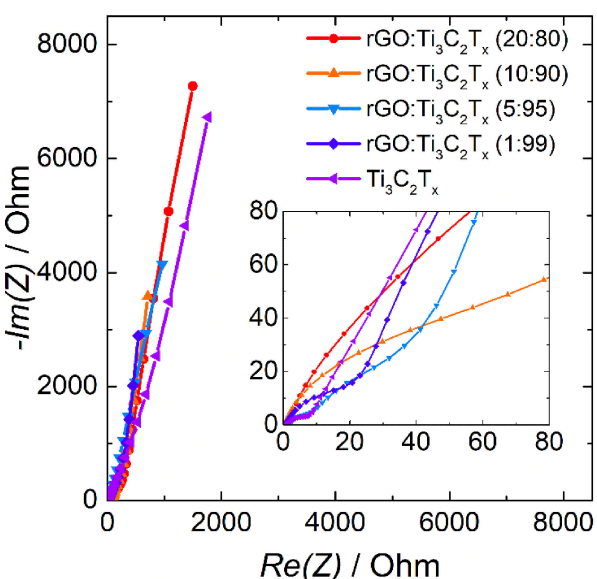


Figure 6. Nyquist plots of the different films presented; inset shows a zoomed in high-frequency region. The increment of the rGO content in the films resulted in an increment of the polarization resistance of the thin film electrodes.

like typical capacitors and the imaginary part of the impedance exhibited a vertical line. However, in the middle frequency range, the effect of the conductivity on the migration rate of the ions into the electrode became more significant and a

Table 1. Electrical conductivity of the films. The error in the film thicknesses values is ~5% due to the surface roughness of the films.

Parameter	0 wt.% rGO	1 wt.% rGO	5 wt.% rGO	10 wt.% rGO	20 wt.% rGO
thickness [μm]	10.0	9.8	10.2	9.9	10.0
conductivity [S cm ⁻¹]	3000 ± 12	2978 ± 28	2764 ± 35	2365 ± 23	2043 ± 29

semicircle appeared.^[32] The diameter of the semicircles of the films increased with the percentage of rGO in the heterostructure, indicating that rGO enhanced the polarization resistance of the electrodes.

The rGO:Ti₃C₂T_x heterostructures were used as electrodes for electrochemical capacitors due to the high electronic conductivity of both materials and an optimal rGO to Ti₃C₂T_x ratio for energy storage applications was determined. The best performance was achieved in the rGO:Ti₃C₂T_x (1:99) film, in which there was approximately 1 layer of rGO for every 18–19 layers of Ti₃C₂T_x. We suggest this was due to the increasing content of rGO flakes relative to the Ti₃C₂T_x flakes and a decrease in the conductivity of the hybrid film compared to pure d-Ti₃C₂T_x. Importantly, the capacitance of the rGO:Ti₃C₂T_x (1:99) and (5:95) films increased compared to that of the pure d-Ti₃C₂T_x, suggesting the beneficial effect from the heterostructure, in agreement with the previously published data.^[19] The possibility of combining MXenes with other 2D materials may expand the applications range of these materials. Particularly, this kind of heterostructures may have superior performance in energy storage devices.^[9]

3. Conclusions

This study demonstrates that heterostructures of rGO and d-Ti₃C₂T_x can be formed by self-assembly, after modifying the functional groups of rGO to make the surface positively charged. We showed that addition of just 1 wt.% of rGO to Ti₃C₂T_x led to an increase in capacitance at low and high scan rates. This work represents a step towards application of rGO and MXene heterostructures in supercapacitors.

Experimental Section

Synthesis of 2D Titanium Carbide MXene

The complete synthesis method for titanium carbide MXene is described elsewhere.^[33] Briefly, to synthesize Ti₃C₂T_x, 20 mL of 9 M hydrochloric acid (HCl, Fisher Scientific) were added to 7.5 molar equivalents (2 g) of lithium fluoride (LiF, Alfa Aesar). The mixture was stirred until the salt was dissolved. Then, 2 g of the ternary titanium aluminum carbide powder (Ti₃AlC₂, <38 µm particle size) were slowly added to the solution. The reaction mixture was held at 35 °C for 24 h while stirring at 200 rpm. After 24 h, the mixture was washed with deionized water and separated by centrifugation at 3500 rpm for two minutes, after which the supernatant was collected. The washing process was repeated until the pH of the supernatant became neutral (pH 6–7). To increase the surface area and delaminate the multilayered powders into single-layer flakes, the Ti₃C₂T_x solution was exposed to bath sonication for 1 h under argon flow. Afterwards, the sonicated solution was centrifuged for another hour at 3500 rpm to separate the single flakes from multilayered flakes. Finally, the supernatant containing single- to few-layer of Ti₃C₂T_x (delaminated Ti₃C₂T_x, d-Ti₃C₂T_x) was collected. This supernatant was used in the preparation of rGO:Ti₃C₂T_x. To prepare a flexible, free-standing d-Ti₃C₂T_x film, the solution was filtered using a polypropylene membrane (3501 Coated PP, Celgard LLC) and dried under vacuum at 120 °C.

Synthesis of NH₂-rGO

The graphite oxide was prepared following the Marcano-Tour method.^[34] The graphite oxide was then sonicated in deionized water for 1 h and the exfoliated graphene oxide (GO) was collected. 210 mg of GO was sonicated in deionized water and 4.5 mL of ethylene-diamine was added to the solution at 600 rpm stirring rate. The reaction continued for 24 h under reflux (80 °C). Finally, aminated reduced graphene oxide (NH₂-rGO) was isolated by centrifugation. The NH₂-rGO was filtered and washed with 500 mL of deionized water. The resulting material was dried in vacuum at 120 °C.

Synthesis of 2D rGO:Ti₃C₂T_x

The NH₂-rGO was sonicated in water to achieve a concentration of 1 mg mL⁻¹. The solutions of NH₂-rGO and d-Ti₃C₂T_x (~17 mg mL⁻¹) were mixed in the desired proportion to achieve 100 mg of rGO:Ti₃C₂T_x (rGO:Ti₃C₂T_x mass proportions: 50:50, 20:80, 10:90, 5:95, 1:99) and shear mixed at 20000 rpm for 10 minutes. To prepare a flexible, freestanding film, the solution was filtered using a polypropylene membrane (3501 Coated PP, Celgard LLC) and dried under vacuum at 120 °C. Vacuum-filtration was conducted with 2 mL of solution and the rest of the solution was kept stirring to avoid re-agglomeration of the particles.

Characterization Methods

To understand the self-assembly process and to quantify the surface charge, zeta (ζ) potential measurements were taken across a pH scale of 2–11. The isoelectric point (IEP) was calculated as the point at which the charge reached a zeta potential of zero mV. ζ -potential was measured on a Malvern Zetasizer Nano ZS (Malvern Instruments, USA) and the pH was changed in situ by titrating known concentrations of acid (0.01 N hydrochloric acid) or base (0.01 N sodium hydroxide) into the solution (MPT-2 Autotitrator).

Characterization of the Ti₃C₂T_x, rGO:Ti₃C₂T_x, and NH₂-rGO film morphologies was carried out using scanning electron microscopy (SEM, Zeiss Supra 50VP, Germany) and composition was determined using energy dispersive x-ray spectroscopy (EDX, Oxford).

Raman spectra were recorded on a Renishaw inVia spectrometer. A 632 nm laser at <1 mW power was focused onto the sample surface through a 60x objective, and the back-scattered light was directed via a 1200 lines/mm diffraction grating to the detector. The interlayer distance of the Ti₃C₂T_x, rGO:Ti₃C₂T_x, and NH₂-rGO films was calculated using x-ray diffraction (XRD). XRD was carried out on a Rigaku Smart Lab (Japan) diffractometer using CuK α radiation (40 kV and 44 mA), a step scan of 0.02 °, 2θ range of 5–50°, and a step time of 0.5 s. Electrical conductivity measurements on a rectangular area of Ti₃C₂T_x and rGO:Ti₃C₂T_x films were obtained by using a digital four-point-probe system (Jandel, England). To obtain reliable electrical conductivity data, five different sites of each film were measured and averaged using the four-point-probe system.

Electrochemical Testing

To quantify the amount of charge stored by the as-prepared materials, all tested films were cut to the same area and weight before being assembled in Swagelok-type cells. The materials were tested in a 3-electrode configuration to evaluate their capacitance and electrochemical stability window. The cells were electrochemically studied by using a 1 M sulfuric acid (H₂SO₄, Sigma Aldrich) electrolyte with a silver/silver chloride (Ag/AgCl) as the reference

electrode. Overcapacitive activated carbon (YP-50, Kuraray) was used as the counter electrode. Cyclic voltammetry (CV) measurements at different scan rates ranging from 2 to 100 mV·s⁻¹ were performed at ambient conditions in a multichannel potentiostat/galvanostat (BioLogic VMP3, France).

Acknowledgements

The authors acknowledge Bilen Akuzum for his help with shear mixing and Tyler Mathis for SEM characterization. A.M.N.S. was supported by CIC energiGUNE, the Basque Government Scholarship for pre-doctoral formation (PRE_2015_2_0096) and the Egonlabur Traveling Grant (EP_2016_1_0030).

Conflict of Interest

The authors declare no conflict of interest.

Keywords: 2D materials • graphene • heterostructure • MXene • supercapacitors

- [1] F. Bonaccorso, L. Colombo, G. Yu, M. Stoller, V. Tozzini, a C. Ferrari, R. S. Ruoff, V. Pellegrini, *Science* **2015**, 347, 1246501.
- [2] L. Wen, J. Chen, J. Liang, F. Li, H. M. Cheng, *Natl. Sci. Rev.* **2017**, 4, 20–23.
- [3] V. Nicolosi, M. Chhowalla, M. G. Kanatzidis, M. S. Strano, J. N. Coleman, *Science* **2013**, 340, 1420–1438.
- [4] M. Naguib, M. Kurtoglu, V. Presser, J. Lu, J. Niu, M. Heon, L. Hultman, Y. Gogotsi, M. W. Barsoum, *Adv. Mater.* **2011**, 23, 4248–4253.
- [5] B. Anasori, M. R. Lukatskaya, Y. Gogotsi, *Nat. Rev. Mater.* **2017**, 2, 16098.
- [6] Y. Wang, H. Dou, J. Wang, B. Ding, Y. Xu, Z. Chang, X. Hao, *J. Power Sources* **2016**, 327, 221–228.
- [7] R. Zhao, M. Wang, D. Zhao, H. Li, C. Wang, L. Yin, *ACS Energy Lett.* **2017**, 132–140.
- [8] M. Yu, S. Zhou, Z. Wang, J. Zhao, J. Qiu, *Nano Energy* **2018**, 44, 181–190.
- [9] E. Pomerantseva, Y. Gogotsi, *Nat. Energy* **2017**, 2, 17089.
- [10] M. Q. Zhao, C. E. Ren, Z. Ling, M. R. Lukatskaya, C. Zhang, K. L. Van Aken, M. W. Barsoum, Y. Gogotsi, *Adv. Mater.* **2015**, 27, 339–345.
- [11] K. Yuan, Y. Xu, J. Uihlein, G. Brunklaus, L. Shi, R. Heiderhoff, M. Que, M. Forster, T. Chassé, T. Pichler, et al., *Adv. Mater.* **2015**, 27, 6714–6721.
- [12] A. C. Ferrari, F. Bonaccorso, V. Falko, K. S. Novoselov, S. Roche, P. Bøggild, S. Borini, F. Koppens, V. Palermo, N. Pugno, et al., *Nanoscale* **2014**, 7, 4598–4810.
- [13] B. Mendoza-Sánchez, Y. Gogotsi, *Adv. Mater.* **2016**, 28, 6104–6135.
- [14] M. R. Lukatskaya, S. Kota, Z. Lin, M.-Q. Zhao, N. Shpigel, M. D. Levi, J. Halim, P.-L. Taberna, M. W. Barsoum, P. Simon, et al., *Nat. Energy* **2017**, 2, 17105.
- [15] X. Zhang, Z. Zhang, Z. Zhou, *J. Energy Chem.* **2017**, 27, 73–85.
- [16] A. M. Navarro-Suárez, K. L. Van Aken, T. Mathis, T. Makaryan, J. Yan, J. Carretero-González, T. Rojo, Y. Gogotsi, *Electrochim. Acta* **2018**, 259, 752–761.
- [17] C. Zhao, Q. Wang, H. Zhang, S. Passerini, X. Qian, *ACS Appl. Mater. Interfaces* **2016**, 8, 15661–15667.
- [18] B. Aïssa, A. Ali, K. A. Mahmoud, T. Haddad, M. Nedil, *Appl. Phys. Lett.* **2016**, 109, 43109.
- [19] J. Yan, C. E. Ren, K. Maleski, C. B. Hatter, B. Anasori, P. Urbankowski, A. Sarycheva, Y. Gogotsi, *Adv. Funct. Mater.* **2017**, 27, 1701264.
- [20] D. Li, M. B. Müller, S. Gilje, R. B. Kaner, G. G. Wallace, *Nat. Nanotechnol.* **2008**, 3, 101–105.
- [21] M. Ghidiu, M. R. Lukatskaya, M.-Q. Zhao, Y. Gogotsi, M. W. Barsoum, *Nature* **2014**, 516, 78–81.
- [22] A. Yasmin, J. L. Abot, I. M. Daniel, *Scr. Mater.* **2003**, 49, 81–86.
- [23] T. W. Healy, D. W. Fuerstenau, *J. Colloid Interface Sci.* **2007**, 309, 183–188.
- [24] A. Sarycheva, T. Makaryan, K. Maleski, E. Satheeshkumar, A. Melikyan, H. Minassian, M. Yoshimura, Y. Gogotsi, *J. Phys. Chem. C* **2017**, 121, 19983–19988.
- [25] T. Hu, J. Wang, H. Zhang, Z. Li, M. Hu, X. Wang, *Phys. Chem. Chem. Phys.* **2015**, 17, 9997–10003.
- [26] A. Ferrari, D. Basko, *Nat. Nanotechnol.* **2013**, 8, 235–46.
- [27] J. Come, Y. Xie, M. Naguib, S. Jesse, S. V. Kalinin, Y. Gogotsi, P. R. C. Kent, N. Balke, *Adv. Energy Mater.* **2016**, 6, 1–9.
- [28] M. R. Lukatskaya, O. Mashtalir, C. E. Ren, Y. Dall'Agnese, P. Rozier, P. L. Taberna, M. Naguib, P. Simon, M. W. Barsoum, Y. Gogotsi, *Science* **2013**, 341, 1502–1505.
- [29] M. Boota, B. Anasori, C. Voigt, M. Q. Zhao, M. W. Barsoum, Y. Gogotsi, *Adv. Mater.* **2016**, 28, 1517–1522.
- [30] D. Wei, Y. Liu, Y. Wang, H. Zhang, L. Huang, G. Yu, *Nano Lett.* **2009**, 9, 1752–1758.
- [31] C.-M. Chen, Q. Zhang, X.-C. Zhao, B. Zhang, Q.-Q. Kong, M.-G. Yang, Q.-H. Yang, M.-Z. Wang, Y.-G. Yang, R. Schlögl, et al., *J. Mater. Chem.* **2012**, 22, 14076.
- [32] P. L. Taberna, P. Simon, J. F. Fauvarque, *J. Electrochem. Soc.* **2003**, 150, A292.
- [33] M. Alhabeb, K. Maleski, B. Anasori, P. Lelyukh, L. Clark, S. Sin, Y. Gogotsi, *Chem. Mater.* **2017**, 29, 7633–7644.
- [34] D. C. Marcano, D. V. Kosynkin, J. M. Berlin, A. Sinitskii, Z. Sun, A. Slesarev, L. B. Alemany, W. Lu, J. M. Tour, *ACS Nano* **2010**, 4, 4806–4814.

Manuscript received: February 25, 2018

Accepted article published: March 26, 2018

Version of record online: April 20, 2018